Journal Name

ARTICLE

Hysteresis and transient behavior in current-voltage measurements of hybrid-perovskite absorber solar cells

E. L. Unger[a*], E. T. Hoke[a,b], C. D. Bailie[a], W. H. Nguyen[c], A. R. Bowring[a], T. Heumüller[a], M. G. Christoforo[d] and M. D. McGehee[a*]

Hybrid organo-metal halide perovskites are an exciting new class of solar absorber materials and have exhibited a rapid increase in solar cell efficiencies throughout the past two years to over 17% in both meso-structured and thin-film device architectures. We observe slow transient effects causing hysteresis in the current-voltage characterization of these devices that can lead to an over- or underestimation of the solar cell device efficiency. We find that the current-voltage (IV) measurement scan direction, measurement delay time, and light and voltage bias conditions prior to measurement can all have a significant impact upon the shape of the measured IV light curves and the apparent device efficiency. We observe that hysteresis-free light IV curves can be obtained at both extremely fast and slow voltage scan rates but only in the latter case are quasi-steady-state conditions achieved for a valid power conversion efficiency measurement. Hysteretic effects are also observed in devices utilizing alternative selective contacts but differ in magnitude and time scale, suggesting that the contact interfaces have a big effect on transients in perovskite-absorber devices. The transient processes giving rise to hysteresis are consistent with a polarization response of the perovskite absorber that results in changes in the photocurrent extraction efficiency of the device. The strong dependence of the hysteresis on light and voltage biasing conditions in thin film devices for a period of time prior to the measurement suggests that photo-induced ion migration may additionally play an important role in device hysteresis. Based on these observations, we provide recommendations for correct measurement and reporting of IV curves for perovskite solar cell devices.

1. Introduction

The rapid increase in hybrid-perovskite solar cell device efficiencies[1–7] are indicative of the tremendous potential of methyl-ammonium lead iodide and related compounds as solar energy absorber materials. Hybrid perovskites have demonstrated high solar energy conversion efficiencies both in thin film device architectures[4,5,8–10] and meso-structured device architectures comprising meso-scopic alumina,[1,3,6] zirconia[11] and titania scaffolds.[2,12,13] It is yet unclear whether perovskite-absorber devices of different architecture types perform equally well or if certain architectures will prove beneficial over others.[12,7] While reported device efficiency values have been sky-rocketing, there has been little debate in the literature about slow transient effects observed in perovskite-absorber devices that severely affect current-voltage measurements from which

device performance metrics are commonly derived.[14–17] Slow transients give rise to hysteresis between IV-measurements performed at different scan rates and directions which can cause both over- and underestimated efficiency values. As for every other new type of solar-absorber material, reliable measurement protocols need to be established to compare device performance metrics between different research laboratories.[18] The power conversion efficiency (η) of a solar cell device is conventionally determined by performing a current-voltage measurement (IV) under standard AM1.5 illumination with a power output of 1000 W m^{-2} ($P_{AM1.5}$). From this measurement, the device performance metrics of open-circuit voltage (V_{OC}), short-circuit current (J_{SC}) and fill factor (FF) are determined. Meaningful device efficiencies can only be derived from IV measurements, if the measurements are carried out under quasi-steady state conditions.[18,19]

Hysteretic effects during IV-measurements have been observed in both mesoscopic[14,16] and thin-film perovskite photovoltaics.[15] In impedance measurements, illuminated perovskite-absorber devices exhibit an additional capacitance at low frequency range[14,20,21] that are caused by slow dynamic processes in the device that cause hysteresis in IV-measurements.[14,16] This distinguishes perovskite-absorber solar cells from solid-state dye-sensitized solar cells that they evolved from. These effects can lead to erroneous device performance metrics if the slow device response is not considered during IV-measurements. Hysteretic phenomena have been observed for other photovoltaic technologies including CIGS, CdTe and amorphous silicon that exhibit high internal capacitances, which have been attributed to charge carrier accumulation in the depletion layer or neutral region of the junction, the existence or formation of defect states and other phenomena such as ion migration.[18,19,22,23] Hysteresis in perovskite-absorber devices has been speculated to originate from trapping/de-trapping of charge carriers,[15,24] changes in absorber or contact conductivity,[25] ferroelectricity[14,15,26,27,28] and ion migration.[29,30,14,15,31,32] Field-dependent orientation effects of the MA^+-dipoles and lattice distortion have been proposed to give rise to polarization effects that affect the charge carrier dynamics.[16,26–28] In addition, metal halides and metal halide perovskites can exhibit significant halide ion mobilities[31,32] that are often accelerated by photoexcitation.[33]

In this report we compare meso-porous titania based perovskite devices to solution-processed thin film devices. Hysteretic effects are observed in both type of architectures. We emphasize that devices may exhibit negligible hysteresis both at fast and slow scan-rates due to a very slow response time. However, perovskite-absorber devices should be measured at a sufficiently slow scan rate that allows for transient processes in the device to settle. A delay time of 5 s before the current is recorded after a change in applied voltage, was found appropriate to determine the device performance of the devices investigated herein. This is approximately equal to a scan rate of 10 mV s^{-1}. Devices with slower response times will need to be measured at even slower scan rates. In this case steady-state power output measurements might be more viable for determining and comparing device efficiencies.[15] Thin film devices exhibit more pronounced hysteresis and also a strong dependence of device performance on bias and illumination conditions before the measurement.

Our experimental observations suggest that multiple processes are responsible for the complex transient behavior in perovskite photovoltaics. The transient currents observed on time scales of a few seconds are consistent with ferroelectric or photoconductive processes. The strong, reversible influence of light and voltage bias pre-conditioning on thin film device performance suggest a mechanism involving ion migration. Due to the strong influence of voltage scan direction, scan rate and device preconditioning on the measured J-V curves of perovskite solar cells, it is essential that authors clearly describe the experimental conditions under which device performance

metrics were derived to allow for comparability between laboratories.

2. Results

2.1. Device fabrication

Meso-porous titania and thin film perovskite-absorber devices were manufactured using similar n-type and p-type selective contacts and only differ in the presence or absence of a meso-porous titania scaffold and the deposition method of the perovskite. Cross-sectional electron microscopy images of representative devices are compared in Figure 1. For both types of devices, the n-type contact comprises a ca. 350-nm-thick fluorine-doped tin oxide layer (F:SnO$_2$) and a ca. 50-nm-thick spray-pyrolyzed compact TiO$_2$ layer. The p-type contact was established by deposition of spiro-OMeTAD doped with 12 mole % spiro-OMeTAD^{2+}(TFSI)$_2$[34] and evaporated gold contacts.

The meso-porous titania-based (mp-TiO$_2$) devices were prepared by first depositing a *ca.* 350-nm-thick meso-porous titania layer followed by a 2-step deposition of the methylammonium lead iodide (MAPbI$_3$) absorber as reported elsewhere.[12] The mp-TiO$_2$/MAPbI$_3$ absorber layer thickness is *ca.* 350 nm (Figure 1 A).

Thin film perovskite devices were prepared by spin-casting solutions containing lead chloride and three equivalents of methylammonium iodide followed by annealing at 100 $^\circ$C in an inert atmosphere as reported elsewhere[1,3,35]. Details of the preparation can be found in the supporting information. The thin film device absorber layer thickness was approximately 400 nm (Figure 1 B).
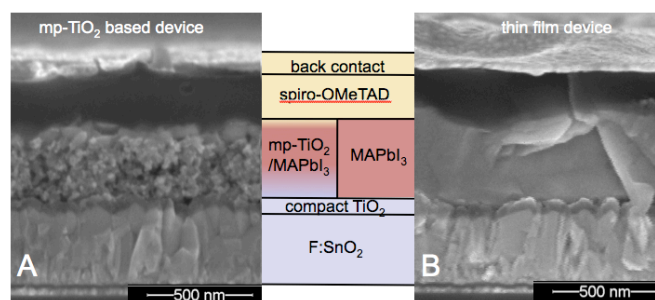

Figure 1: Cross-sectional scanning-electron microscope images of different perovskite-absorber device architectures comprising methylammonium lead iodide (MAPbI$_3$). (A) Meso-porous titanium dioxide (mp-TiO$_2$) based-device and (B) solution-processed thin film device. The colored schematic illustrates the PIN architecture of both types of devices.

2.2. Hysteresis in current-voltage measurements

We found that the device performance metrics derived from current-voltage measurements crucially depend on the scan direction and delay time after each voltage step before the measurement is taken. In Figure 2, IV-curves were measured with either a 10 ms or 5 s delay after each 50 mV voltage step.
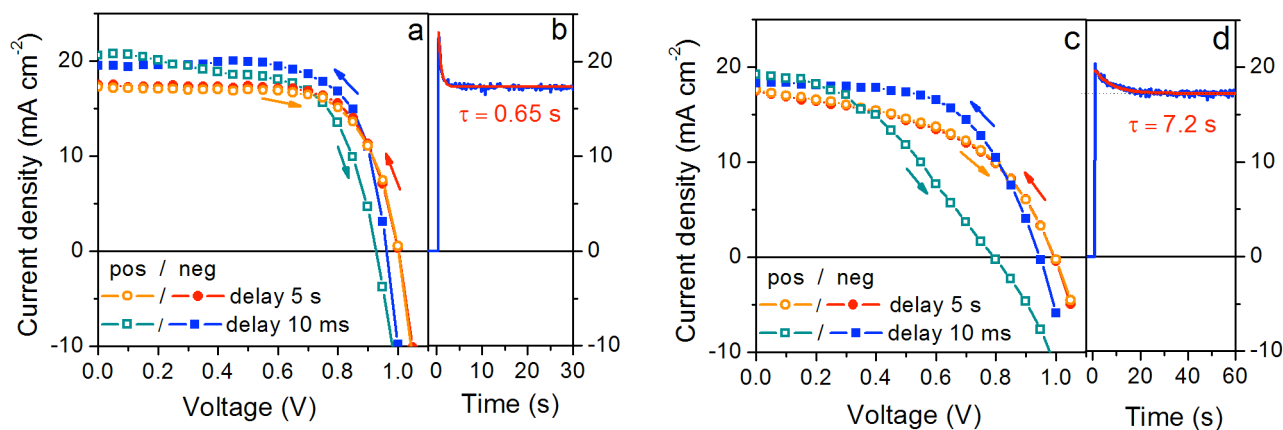
Figure 2 Current-voltage measurements of mesoporous-TiO$_2$ based perovskite-absorber device (a) and thin film device (c). Different scan directions (pos: 0V to forward bias, neg: forward bias to 0V) and delay times (0.01 s for fast scan and 5 s for slow scan) are compared. (b & d) Corresponding short-circuit current transients when switching the devices from V$_{OC}$ to J$_{SC}$ during illumination.

Table 1: Comparison of device efficiency metrics for different delay times (10 ms vs 5 s) and scan directions (pos: J$_{SC}$ to V$_{OC}$, neg: V$_{OC}$ to J$_{SC}$)									
		mp-TiO$_2$-based device				**thin film device**			
Delay time (sec)	**Scan direction**	**J$_{SC}$ (mA cm^{-2})**	**V$_{OC}$ (V)**	**FF**	**P$_{max}$ (%)**	**J$_{SC}$ (mA cm^{-2})**	**V$_{OC}$ (V)**	**FF**	**P$_{max}$ (%)**
0.01	pos	20.6	0.93	0.62	11.9	19.2	0.79	0.40	6.07
0.01	neg	20.0	0.96	0.71	13.6	18.8	0.92	0.65	11.2
5	pos	17.2	1.00	0.70	12.2	17.6	1.00	0.49	8.62
5	neg	17.2	1.01	0.72	12.4	17.5	1.00	0.48	8.40

The measurement delay time is a more relevant metric than the scan rate because it can be directly compared to the device settling time for the various transient processes that will be discussed later. Delay times of 10 ms and 5 s are equivalent to scan rates of *ca.* 2 V s^{-1} and 10 mV s^{-1} (Table S1). The scans for both positive (i.e. J$_{SC}$→V$_{OC}$, ΔV = 50 mV) and negative (i.e. V$_{OC}$→J$_{SC}$, ΔV = -50 mV) directions and the device performance metrics derived from these measurements are compared in Table 1. Prior to each measurement the devices were kept at illumination under open circuit conditions.

At a short delay time of 10 ms, significant hysteresis is observed for both the mp-TiO$_2$ based devices (Figure 2a) and the thin film devices (Figure 2c). For the mp-TiO$_2$ based device shown in Figure 2a, the efficiency at a 5 s delay time is 12.3 % but would be overestimated to be 13.6 % when measured with 10 ms delay time in the negative scan direction or underestimated to be 11.9 % when measured rapidly in the positive scan direction. This agrees with the slow time-constant hysteretic phenomena observed in impedance measurements by Dualeh et al.[14] For the thin film device, measurement at 10 ms delay time in the negative direction results in an 11.2 % device efficiency, while the scan in the opposite direction yields a power conversion efficiency of 6.07 %. At a delay time of 5 s, the positive and negative scans converge with an efficiency of 8.5 ± 0.1 %.

The meso-porous titania based devices exhibited less hysteresis and a weaker dependence of the device efficiency on the measurement delay time compared to the thin-film devices. The meso-scopic devices exhibited an apparent reverse-scan efficiency of 12.5% and 11.3%, using a delay time of 10 ms and 5 s, respectively (Figure S2). For the thin film devices

investigated, the average device efficiency between a fast scan and slow scan in the negative scan direction was 10.1% *vs.* 6.7% (Figure S2).

The conditions immediately prior to the IV-scan have a significant impact on the IV-measurements of perovskite-absorber solar cells. The IV-curves measured at fast scan-rates for the mp-TiO$_2$ based device (Figure 2a) exhibit higher photocurrents in the initial phase of the scan both in the negative and positive direction. This can be most clearly seen in the negative direction scan (blue) where the measured current density at 0.6 V is actually higher than at J$_{SC}$. We found this to be a consequence of devices being held at open-circuit conditions and illumination for about 3 seconds immediately prior to the measurements. To illustrate this, we measured the current response of devices switched from open-circuit to short circuit under illumination. Both for mp-TiO$_2$ based (Figure 2b) and thin film devices (Figure 2d) the photocurrent initially reaches values above 20 mA/cm^2 but decays to about 17 mA/cm^2 over time. This agrees well with the J$_{SC}$ determined at long delay times (Table 1). The fit of the transients to a mono-exponential decay yields time constants of 0.65 s and 7.2 s for the mp-TiO$_2$ and thin film device, respectively. Thin film devices exhibit a much slower response.

The absence of hysteresis in IV-measurements is not sufficient evidence to ensure that devices are measured under quasi-steady-state conditions. When devices are measured in either positive or negative scan direction after being held at open-circuit conditions immediately prior to the IV-measurement they may appear hysteresis-free at very fast scan-rates, which we demonstrate for a meso-porous titania-based device in Figure 3.
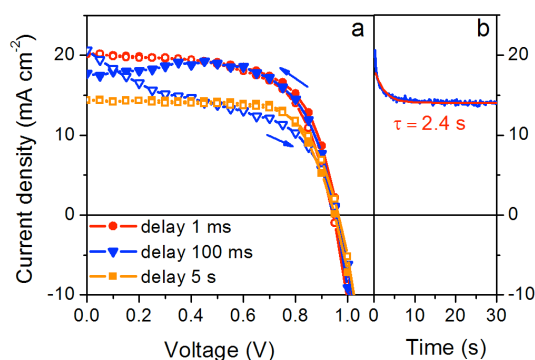
Figure 3 Meso-porous titania based perovskite-absorber device with no IV-hysteresis at very fast and slow scan-rates.

This device does not exhibit hysteresis between the positive and negative IV-scan direction at very short delay times of 1 ms (see table S1 for equivalent scan rate) nor at long delay times of 5 s, which equals about 10 mV s^{-1}. At intermediate delay times of 100 ms the IV-scans in the positive and negative scan direction do not match. The device efficiency derived from the hysteresis-free IV-measurements at fastest and slowest scan rate is 12.3 vs 9.7%.

The IV-measurement can be rationalized by over-laying the IV-measurement at long delay times with an exponentially decaying current shown in Figure S3. The shape of the IV-curves is not typical for hysteretic device behavior but a consequence of the devices being held at forward bias and illumination immediately prior to the IV-measurements. An IV-measurement at fast scan-rates performed in a cyclic fashion exhibits typical hysteretic behavior (Figure S2). The resulting IV-traces are similar to the experimental data and also predict that no hysteresis is expected for very fast scan rates as the transient photocurrent would not have settled during the course of the scan. We observe very similar results for thin film devices (Figure S4).

As perovskite-absorber device exhibit slow transient effects, it is more meaningful to compare the performance of perovskite-absorber solar cells by measuring the power generated by the device over time. In Figure 4, we show the efficiency of the devices compared in Figure 2. The efficiency was derived by measuring the current over time at a constant potential close to the maximum power point determined from IV-measurements at slow scan-rates shown in Figure 2.

In this particular case, the light source was periodically turned on and off. During cyclic illumination, the thin film devices was found to give a fairly consistent power conversion efficiency of close to 8%. Under constant illumination the photocurrent of thin film devices was found to slowly decrease (Figure S5) which will be further discussed in sections 2.3 and 2.5. The meso-porous titania-based devices had a stable efficiency of 12% which is comparable to the device performance data derived from IV-measurements at long delay times of 5 s.
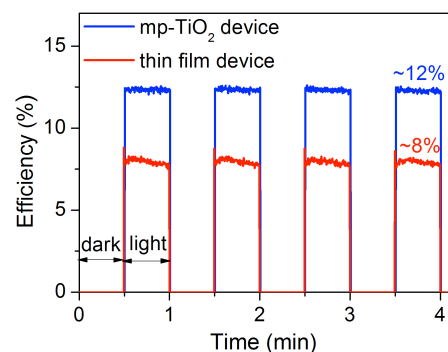

Figure 4: Comparison of conversion efficiency of devices of different architectures during in response to dark-light illumination conditions

2.3. Slow transients in EQE measurements

External quantum efficiency (EQE) measurements are commonly carried out under short-circuit conditions, and integration of the EQE with respect to the AM1.5G spectrum should amount to a similar current density as determined from IV-measurements. The integrated EQE amounts to 17.3 mA cm^{-2} (Figure 5a) which agrees well with the short-circuit photocurrent density determined from IV-measurements at long delay times (Figure 2a) and the steady-state photocurrent (Figure 5b).
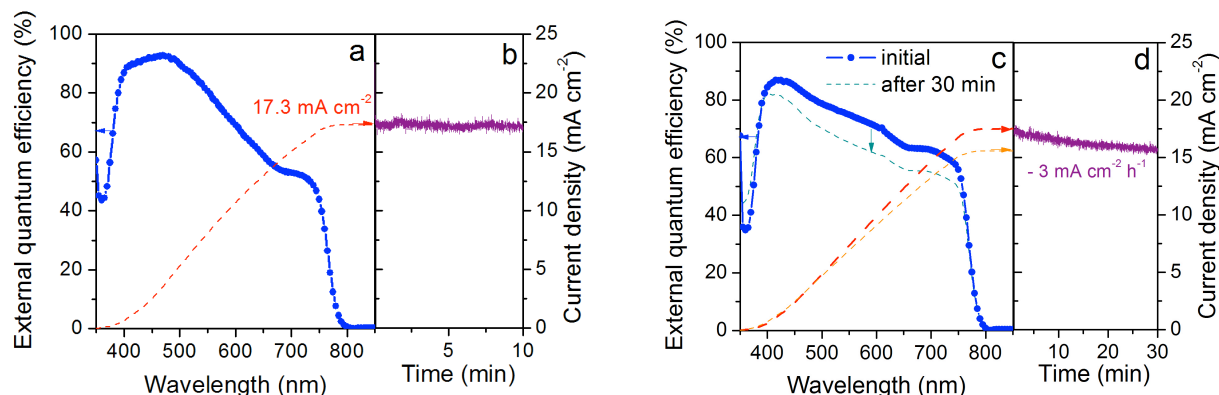

Figure 5 External quantum efficiency measurements of (a) meso-porous titania and (c) thin film perovskite absorber devices. (b & d) show the short circuit photocurrent density (J_{SC}) transient on a longer time-scale. The J_{SC} steadily decreases for the thin film device in a linear fashion reflected in a decrease in EQE and integrated photocurrent while the J_{SC} of the mp-TiO₂-based device remains fairly stable.
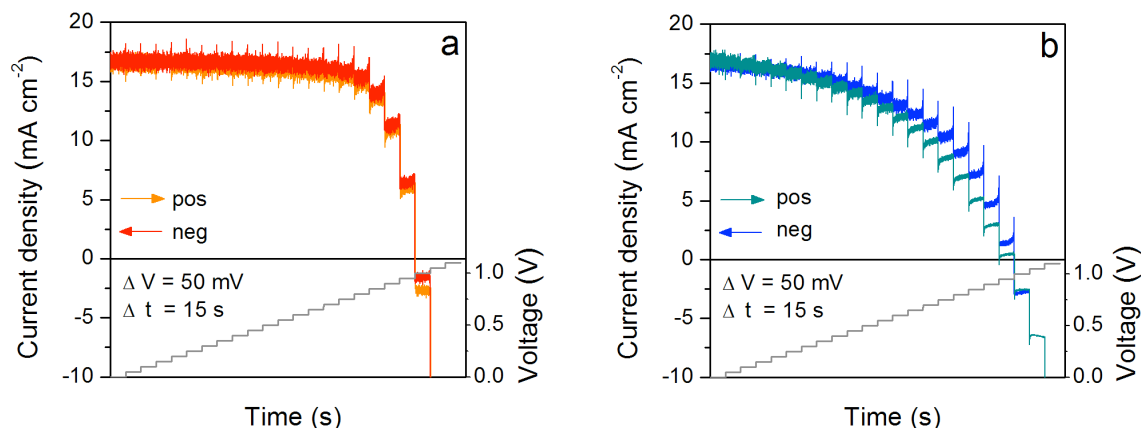
Figure 6 Step-wise current voltage measurement illustrating the effect of delay time after voltage step on IV-curve due to capacitive effects in the device (a) for an mp-TiO$_2$ based device and (b) for a thin film device. The voltage steps were 50 mV and 15 s long for both directions but a unit-less time axis was used to compare the plots to each other.

The EQE and integrated EQE of the thin film device is shown in Figure 5c. The first measurement was performed after having light-soaked the device for 5 minutes at forward bias. The EQE integrates to 17.4 mA cm^{-2} which matches the short-circuit photocurrent density (J$_{SC}$) determined by IV-measurement at long delay times (Figure 2 c).

When measured several times consecutively, the EQE and hence photocurrent determined from the integrated EQE decreases. The steady-state short-circuit photocurrent density J$_{SC}$ decayed at a rate of ca 3 mA cm^{-2} per hour. This photocurrent decay can result in systematic distortions of the EQE spectral shape if the photocurrent has decreased appreciably over the time it takes to perform a spectral scan. (Figure S6).

The spectral shape of the EQE did not change substantially between repeated scans, suggesting that the photocurrent decay results from a reduction in the charge extraction efficiency rather than optical changes to the absorber or contact layer. These slow transients make it difficult to match integrated EQE values with photocurrent densities determined from IV-measurements at long delay times or steady-state photocurrent measurements. The decrease in photocurrent is reversible, which will be further discussed in section 2.5.

2.4. Step-wise IV-measurements

To illustrate the importance of measurement delay time after each voltage step in IV-measurements, we performed step-wise, time resolved, I-V measurements. The voltage was changed in 50 mV increments in either the positive (+ 50 mV) or negative (-50 mV) scan direction and the current was continuously recorded *vs.* time. Prior to the measurement devices were kept at the starting voltage for 1 minute under illumination. These measurements are shown in Figure 5 (a) and (b) for the mp-TiO$_2$ and thin film device, respectively. After each voltage step, the current response exhibits a spike followed by an exponential decay or rise when scanning in the negative or positive direction, respectively. These transient effects give rise to a lower apparent photocurrent for the

positive and a higher apparent photocurrent for the negative scan direction. The delay time after each voltage step therefore should be long enough to allow for transient effects to settle and depends on the response time of the device under investigation. For both type of architectures investigated herein a delay time of at least 5 s, equivalent of a scan rate of ~10 mV s^{-1} (Table S1), was found appropriate. For the thin film device the time resolved IV-measurements reveal that maybe even longer delay times would be appropriate as there is a discrepancy at higher applied potentials between the scans. These effects are due to transients on a very long time scale induced in the device during light-soaking at different bias, which will be discussed further in section 2.5.

Light appears to play an important role in the transient processes that cause hysteretic effects during IV-measurements. For step-IV measurements in the dark, the transient current response was observed to be orders of magnitude lower, especially at low bias voltages and currents (Figure S7). Light soaking prior to the measurement also influences the magnitude of the photocurrent transients and the delay time. (Figure S8).

The dependence of transient currents on scan direction as shown in Figure 6 is suggestive of perovskite-absorber devices exhibiting a large effective capacitance in the light. Summation of integrated current transients during each voltage step in the step-IV measurements (Figure 6b) yields a charge density on the order of 10^{-2} C cm^{-2}. A similar charge density is obtained from integrating the current transient observed from switching the device from V$_{OC}$ to J$_{SC}$ in a single step (Figure 5d). This charge density is too large to originated from accumulated charge carriers in the device, which would require a dielectric constant of ε_r ~5x10^6 or unrealistically high carrier densities of ~10^{21} cm^{-3}. We hypothesize that the large effective capacitance of perovskite solar cells under illumination is caused by the ferroelectric response of perovskite, amplified by photoconductive effects. Very recently it has been reported that MAPbI$_3$ exhibits an extremely large dielectric constant on the order of ε_r ~10^3, and exhibits an effective dielectric constant that can be 1000 times higher under illumination.[36] The

perovskite ferroelectric response was attributed to structural rearrangement originating from reorientation of methylammonium ions (MA$^+$). We suggest that polarization of the perovskite may influence the charge carrier extraction efficiency from the device, giving rise to the observed photocurrent transients and consequently hysteretic effects.

For the thin film device, the transient current does not appear to reach a steady-state value during the time interval of 15 s at applied potentials of ~0.6 V and the scans in the positive and negative directions differ substantially from each other. These observations suggest that there may be an additional slower transient process that could be of different origin than the transients observed in the second time range. These will be discussed further in the next section.

2.5. Effect of light-soaking at different bias

Hitherto, there has been little discussion about the effect and importance of pre-conditioning steps for perovskite-absorber devices, such as light-soaking at forward bias[15]. We find that the conditions prior to the IV-measurement have a huge effect on the performance of thin film devices. After storage in the dark and prior to any light-soaking, thin-film devices often exhibited IV curves with a slight s-shape and rather low

performance as shown in Figure 7a. Light-soaking at far-forward bias conditions (J>0) dramatically improved the fill factor and photocurrent of this device leading to a power conversion efficiency increase from about 2% to about 4%. For some devices, such as for the one shown in Figure 7, we were able to further improve the device efficiency to about 7% by cycling the device between forward bias and 0V under illumination several times prior to performing the IV-measurement. Illumination under reverse bias conditions where the current flows in the opposite direction had the opposite effect causing the IV-curves to become more s-shaped over time and the photocurrent to decrease. This can explain the slow decrease in short-circuit photocurrent with time discussed in section 2.3 (Figure 5d) where the current also flows in a negative direction. We found that we repeatedly improve or diminish the device efficiency by cycling the voltage bias conditions during light soaking, indicating that there are reversible processes occurring in perovskite-absorber solar cells. In contrast, meso-porous titania based devices performed fairly independently of illumination and bias conditions prior to the measurements (Figure S9).
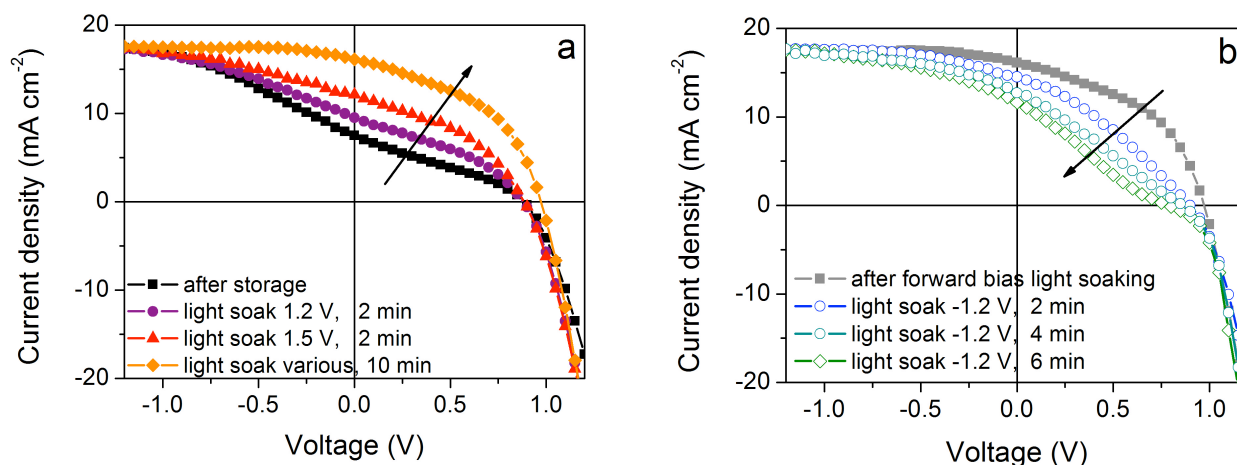

Figure 7 (a) Effect of light-soaking under forward bias conditions on the IV-behavior of a thin film perovskite device. (b) Effect of light-soaking under reverse bias conditions on the IV-behavior of the same device. These results suggest reversible photo-induced ion migration processes occuring in the device under operation. A delay time of 5 s was chosen for the scans equivalent of a scan rate of 10 mV s^{-1}.

3. Discussion

We have demonstrated that transient effects in perovskite-absorber solar cells can lead to an overestimation of the device performance, if the device is measured rapidly after light-soaking at open-circuit or forward bias conditions (Sections 2.2 and 2.3). These effects are observed both for meso-porous titania based devices as well as thin film devices, in agreement with other reports.[14,15] The appropriate scan rate for the IV-characterization of a solar cell devices depends on the time constant of these transient effects in the current. While 10 mV s^{-1} was found to be an appropriate scan rate for the devices

investigated herein, longer delay times might have to be used for other perovskite-absorber solar cells.

In comparison, solution-processed thin film devices exhibit a larger discrepancy between the performance determined at short vs. long delay times in current-voltage measurements (Figure 2 c & S2). The comparison of hysteretic effects observed for thin film devices with meso-porous titania based devices suggests that the transients are not caused by interfacial trap states as in this case meso-porous mp-TiO$_2$ based devices would be expected to exhibit more pronounced hysteretic effects. The meso-porous titania based devices exhibit faster transients which may be rationalized with the titania scaffold providing efficient pathways for electron extraction as well as

limiting the growth and size perovskite crystals. Both factors can be expected to affect the polarizability and long-range charge carrier and ionic transport within the perovskite absorber.

The transient processes responsible for hysteresis appear to originate from the processes in the bulk of the perovskite-absorber. We have observed hysteresis in all of the perovskite device architectures that we have examined, irrespective of contact materials. When omitting the spiro-OMeTAD from our devices and contacting the perovskite-absorber directly with gold, hysteresis persisted (Figure S10 b). This suggests that hysteretic effects are neither solely caused by the perovskite/spiro-OMeTAD interface nor diffusion of Li^+, introduced to the device with the hole-transporting medium. We have found that contacts can influence the size and direction of the transients and hysteresis. Inverted thin film devices using PEDOT:PSS and $PC_{60}BM$ as hole and electron-selective contacts exhibit hysteresis at fast scan rates but the photocurrent appears to be lower rather than higher at fast scan rates (Figure S10 a). These observations are consistent with a mechanism where transient polarization of the perovskite absorber results in changes in charge carrier extraction efficiency at the carrier-selective contacts. In inverted devices, we found the photocurrent not to be as dependent on IV-scan delay time. This suggests that the charge extraction efficiency is not as severely affected by changes in perovskite polarization in these type of devices.

It is not yet clear whether the current transients in response to changes in the applied voltage have a similar origin to the slower processes occurring during pre-conditioning of the devices. The strong influence of bias pre-conditioning on IV measurements suggests that polarization-induced changes in the device may play an important role in the observed current transients and device hysteresis. This polarization could be caused by diffusion of ionic species[14,15,28,31,32] or alignment of methylammonium dipoles within the metal-halide lattice[14,15,26–28] under an applied voltage bias, resulting in changes in ability for photocurrent to be extracted from the device. Recent impedance studies on perovskite-absorber solar cells analyzing low-frequency phenomena observed slow transients with similar time-constants as the effects described in section 2.2. and 2.4.[16] They arrive at a similar conclusion, that the observed transiently higher photocurrent cannot be explained by charge-carrier accumulation but is likely due to ferroelectric MA^+ re-orientation and lattice distortion effects giving rise to polarized domains.

We propose that ion migration may also play a role in slower processes occurring during pre-conditioning of the devices. We suggest that photo-excitation of $MAPbI_3$ may enhance the ionic conductivity of the material, resulting in the observed transient currents and hysteresis when a bias is applied to the device. This process is well known to occur in metal halides, including PbI_2 where photo-excitation creates halide vacancies that enable the migration of halide ions.[33] Once these vacancies are created, an applied external bias can result in a redistribution of ions within the device, producing electric fields that aid or counteract charge carrier extraction. This can explain why under continuous illumination, the external quantum efficiency (Figure 5 c) and photocurrent (Figure 5 d) slowly decreases in perovskite solar cells and why applying a large forward bias to reverse the current direction causes the photocurrent to recover. Applying a reverse bias or short circuit conditions during illumination is expected to cause negatively charged ions such as I^- in the perovskite to migrate towards the titania cathode and positive ions such as MA^+ and Li^+ towards the hole-selective contact. This may create an extraction barrier for both electrons and holes at their respective contact, resulting in the observed s-shaped IV behavior (Figure 7). Forward-biasing the device during illumination can drive these ions in the opposite direction, potentially allowing the device photocurrent to recover if the pre-conditioning forward bias is applied for an adequate time. This redistribution of ions under illumination can explain why the current-voltage behavior of perovskite devices is sensitive to the pre-conditioning bias history before the measurement, as discussed in section 2.5.

Since ion migration is particularly sensitive to the concentration of mobile vacancies (or interstitials depending on the mechanism), this proposed mechanism would suggest that the transient behavior of perovskite devices should be influenced by the precise stoichiometry of the perovskite material, as well as the degree of crystallinity and the size of crystalline domains. The significant differences in the transient behavior that we observed between the meso-scopic and thin-film devices may be a consequence of differences in stoichiometry or morphology due to the differences in processing. The thin films devices may contain trace amounts chloride due to the employed deposition procedure. As any ion migration will likely be detrimental for the long-term reliability of perovskite-absorber devices, reducing any ion-migratory effects in hysteresis may be an important step for improving long-term reliability.

4. Conclusion & Outlook

We find that transient phenomena heavily influence the current-voltage characteristics of perovskite-absorber solar cells. To allow for comparison of device efficiencies between research laboratories, preconditioning, scan rates and directions at which IV-measurements were performed should be reported as all the factors may have a huge impact on device performance metrics. Reports on perovskite-absorber device performance should include a discussion about hysteretic effects as optimization of perovskite-absorber processing or selective contacts may increase or reduce hysteretic effects. The absence of hysteresis between IV-scans in different scan directions is not sufficient to verify that IV-measurements are carried out under quasi-steady state conditions as transient effect may occur on time scales slower than the scan rate. The steady-state maximum power output of a device over time should be measured and reported, if performance metrics determined from IV-measurements are ambiguous. External

quantum efficiency measurements are a valuable point of reference as these are usually carried out under steady-state conditions.

More research needs to be undertaken to understand how the unique properties of this novel family of solar absorber materials give rise to e.g. long charge carrier lifetimes[37,38] and mobility.[39,40] The same properties may also cause the transient and hysteretic effects discussed herein and it will be crucial to understand how they will affect the long-term reliability of perovskite-absorber devices. In the optimization of different device architectures and selective contact materials for organo-metal halide perovskites, the investigation of hysteretic and transient effects will prove a valuable tool.

Acknowledgements

Notes and references

a Department of Materials Science and Engineering

b Geballe Laboratory for Advanced Materials

c Department of Chemistry

d Department of Electrical Engineering,

Stanford University, Stanford, CA 94305, USA

Corresponding Authors:

M. D. McGehee, e-mail:mmcgehee@stanford.edu

E. L. Unger, e-mail: eva.unger@chemphys.lu.se

1. M. M. Lee, J. Teuscher, T. Miyasaka, T. N. Murakami, and H. J. Snaith, *Science*, 2012, **338**, 643–7.
2. H.-S. Kim, C.-R. Lee, J.-H. Im, K.-B. Lee, T. Moehl, A. Marchioro, S.-J. Moon, R. Humphry-Baker, J.-H. Yum, J. E. Moser, M. Grätzel, and N.-G. Park, *Sci. Rep.*, 2012, **2**, 591.
3. J. M. Ball, M. M. Lee, A. Hey, and H. J. Snaith, *Energy Environ. Sci.*, 2013, **6**, 1739.
4. M. Liu, M. B. Johnston, and H. J. Snaith, *Nature*, 2013, **501**, 395–8.
5. D. Liu and T. L. Kelly, *Nat. Photonics*, 2013, **8**, 133–138.
6. J. T.-W. Wang, J. M. Ball, E. M. Barea, A. Abate, J. A. Alexander-Webber, J. Huang, M. Saliba, I. Mora-Sero, J. Bisquert, H. J. Snaith, and R. J. Nicholas, *Nano Lett.*, 2014, **14**, 724–30.
7. *N.R.E.L (NREL), Best Res. Effic*.
8. G. E. Eperon, S. D. Stranks, C. Menelaou, M. B. Johnston, L. Herz, and H. Snaith, *Energy Environ. Sci.*, 2014, **7**, 982–988.
9. J. You, Z. Hong, Y. M. Yang, Q. Chen, M. Cai, T.-B. Song, C.-C. Chen, S. Lu, Y. Liu, H. Zhou, and Y. Yang, *ACS Nano*, 2014, **8**, 1674–1680.
10. Q. Chen, H. Zhou, Z. Hong, S. Luo, H.-S. Duan, H.-H. Wang, Y. Liu, G. Li, and Y. Yang, *J. Am. Chem. Soc.*, 2014, **136**, 622–5.
11. D. Bi, S.-J. Moon, L. Häggman, G. Boschloo, L. Yang, E. M. J. Johansson, M. K. Nazeeruddin, M. Grätzel, and A. Hagfeldt, *RSC Adv.*, 2013, **3**, 18762.
12. J. Burschka, N. Pellet, S.-J. Moon, R. Humphry-Baker, P. Gao, M. K. Nazeeruddin, and M. Grätzel, *Nature*, 2013, **499**, 316–9.
13. N. Pellet, P. Gao, G. Gregori, T.-Y. Yang, M. K. Nazeeruddin, J. Maier, and M. Grätzel, *Angew. Chem. Int. Ed. Engl.*, 2014, **53**, 3151–7.
14. A. Dualeh, T. Moehl, N. Tétreault, J. Teuscher, P. Gao, M. K. Nazeeruddin, and M. Grätzel, *ACS Nano*, 2014, **8**, 362–373.
15. H. J. Snaith, A. Abate, J. M. Ball, G. E. Eperon, T. Leijtens, N. K. Noel, S. D. Stranks, J. T.-W. Wang, K. Wojciechowski, and W. Zhang, *J. Phys. Chem. Lett.*, 2014, **5**, 1511–1515.
16. R. S. Sánchez, V. Gonzalez-Pedro, J.-W. Lee, N.-G. Park, Y. S. Kang, I. Mora-Sero, and J. Bisquert, *J. Phys. Chem. Lett.*, 2014, 140618175931007.
17. R. Gottesman, E. Haltzi, L. Gouda, S. Tirosh, Y. Bouhadana, A. Zaban, E. Mosconi, and F. De Angelis, *J. Phys. Chem. Lett.*, 2014, 140722203534006.
18. J. A. del Cueto, C. A. Deline, D. S. Albin, S. R. Rummel, and A. Anderberg, *Proc. SPIE 7412, Reliab. Photovolt. Cells, Modul. Components, Syst. II*, 2009, 741204.
19. M. Herman, M. Jankovec, and M. Topic, *Int. J. Photoenergy*, 2012, **2012**, 151452.
20. H.-S. Kim, I. Mora-Sero, V. Gonzalez-Pedro, F. Fabregat-Santiago, E. J. Juarez-Perez, N.-G. Park, and J. Bisquert, *Nat. Commun.*, 2013, **4**, 2242.
21. V. Gonzalez-Pedro, E. J. Juarez-Perez, W.-S. Arsyad, E. M. Barea, F. Fabregat-Santiago, I. Mora-Sero, and J. Bisquert, *Nano Lett.*, 2014, **14**, 888–93.
22. D. S. Albin and J. A. del Cueto, in *2010 IEEE International Reliability Physics Symposium*, IEEE, 2010, pp. 318–322.
23. C. Monokroussos, R. Gottschalg, A. N. Tiwari, G. Friesen, D. Chianese, and S. Mau, in *2006 IEEE 4th World Conference on Photovoltaic Energy Conference*, IEEE, 2006, vol. 2, pp. 2231–2234.
24. T. Heiser and E. Weber, *Phys. Rev. B*, 1998, **58**, 3893–3903.
25. D. L. Staebler and C. R. Wronski, *J. Appl. Phys.*, 1980, **51**, 3262.
26. J. M. Frost, K. T. Butler, F. Brivio, C. H. Hendon, M. van Schilfgaarde, and A. Walsh, 2014, **14**, 2584–2590.
27. F. Brivio, A. Walker, and A. Walsh, *APL Mater.*, 2013, **1**, 042111.
28. C. C. Stoumpos, C. D. Malliakas, and M. G. Kanatzidis, *Inorg. Chem.*, 2013, **52**, 9019–38.
29. I. Lyubomirsky, M. K. Rabinal, and D. Cahen, *J. Appl. Phys.*, 1997, **81**, 6684.
30. D. S. Albin, R. G. Dhere, S. C. Glynn, J. A. del Cueto, and W. K. Metzger, in *SPIE Solar Energy + Technology*, eds. N. G. Dhere, J. H. Wohlgemuth, and D. T. Ton, International Society for Optics and Photonics, 2009, p. 74120I–74120I–12.
31. J. Mizusaki, K. Arai, and K. Fueki, *Solid State Ionics*, 1983, **11**, 203–211.
32. K. Yamada, K. Isobe, E. Tsuyama, T. Okuda, and Y. Furukawa, *Solid State Ionics*, 1995, **79**, 152–157.
33. J. F. Verwey, *J. Phys. Chem. Solids*, 1970, **31**, 163–168.
34. W. H. Nguyen, C. D. Bailie, E. L. Unger, and M. D. McGehee, *J. Am. Chem. Soc.*, 2014, online, July 22.
35. G. E. Eperon, V. M. Burlakov, P. Docampo, A. Goriely, and H. J. Snaith, *Adv. Funct. Mater.*, 2014, **24**, 151–157.
36. E. J. Juárez-Pérez, R. S. Sánchez, L. Badia, G. Garcia-Belmonte, Y. S. Kang, I. Mora-Sero, and J. Bisquert, *J. Phys. Chem. Lett.*, 2014, 140623103539001.
37. S. D. Stranks, G. E. Eperon, G. Grancini, C. Menelaou, M. J. P. Alcocer, T. Leijtens, L. M. Herz, A. Petrozza, and H. J. Snaith, *Science*, 2013, **342**, 341–4.

38.   G. Xing, N. Mathews, S. Sun, S. S. Lim, Y. M. Lam, M. Grätzel, S. Mhaisalkar, and T. C. Sum, *Science*, 2013, **342**, 344–7.
39.   A. Marchioro, J. Teuscher, D. Friedrich, M. Kunst, R. Van De Krol, T. Moehl, and M. Gratzel, *Nat. Photonics*, 2014, 1–6.
40.   C. S. Ponseca, T. J. Savenije, M. A. Abdellah, K. Zheng, A. P. Yartsev, T. Pascher, T. Harlang, P. Chabera, T. Pullerits, A. Stepanov, J.-P. Wolf, and V. Sundstrom, *J. Am. Chem. Soc.*, 2014, 140321162357007.